

# MegaSR: Mining Customized Semantics and Expressive Guidance for Image Super-Resolution

Xinrui Li<sup>1</sup> Jianlong Wu<sup>1</sup> Xinchuan Huang<sup>2</sup> Chong Chen<sup>2</sup>  
 Weili Guan<sup>1</sup> Xian-Sheng Hua<sup>2</sup> Liqiang Nie<sup>1</sup>

<sup>1</sup>Harbin Institute of Technology, Shenzhen <sup>2</sup>Terminus Group

felix.leeovo7@gmail.com, wujianlong@hit.edu.cn, huangxch26@mail2.sysu.edu.cn  
 chenchong.cz@gmail.com, guanweili@hit.edu.cn, huaxiansheng@gmail.com, nieliqiang@gmail.com

<https://github.com/striveAgain/MegaSR>

## Abstract

Pioneering text-to-image (T2I) diffusion models have ushered in a new era of real-world image super-resolution (Real-ISR), significantly enhancing the visual perception of reconstructed images. However, existing methods typically integrate uniform abstract textual semantics across all blocks, overlooking the distinct semantic requirements at different depths and the fine-grained, concrete semantics inherently present in the images themselves. Moreover, relying solely on a single type of guidance further disrupts the consistency of reconstruction. To address these issues, we propose MegaSR, a novel framework that mines customized block-wise semantics and expressive guidance for diffusion-based ISR. Compared to uniform textual semantics, MegaSR enables flexible adaptation to multi-granularity semantic awareness by dynamically incorporating image attributes at each block. Furthermore, we experimentally identify HED edge maps, depth maps, and segmentation maps as the most expressive guidance, and propose a multi-stage aggregation strategy to modulate them into the T2I models. Extensive experiments demonstrate the superiority of MegaSR in terms of semantic richness and structural consistency.

## 1. Introduction

Image super-resolution (ISR), a critical field in low-level computer vision, aims to reconstruct high-resolution (HR) images from degraded low-resolution (LR) counterparts. Primarily, ISR faces two key challenges: (1) The complex nonlinear mapping renders traditional methods ineffective; (2) Diverse LR observations further complicate reconstruction. Deep learning-based methods have significantly advanced ISR by leveraging the powerful capabilities of deep networks to model complex distributions. Early research [12, 14, 28, 35, 49, 81] trains deep networks on

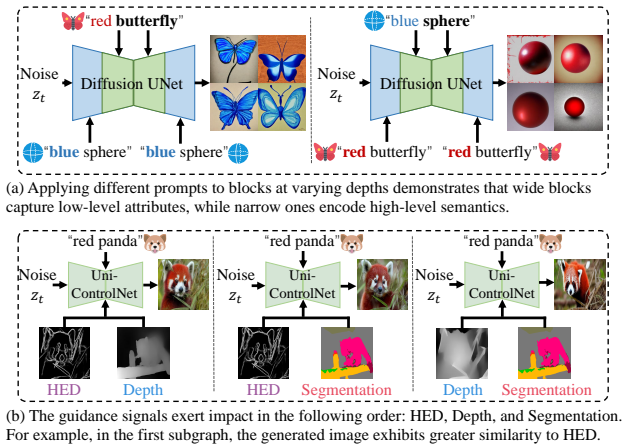


Figure 1. The motivation of MegaSR. (a) We apply different prompts to blocks at varying depths to explore the depth-specific representations of the diffusion unet. (b) We utilize paired guidance signals with consistent semantics but opposing structures to evaluate their relative impact.

synthetic LR-HR pairs generated by predefined degradations, but the fidelity-focused objectives often result in over-smoothed outcomes. To address this, Generative Adversarial Networks (GANs) [16] are introduced to enhance perceptual quality through adversarial learning. Despite their potential, GANs suffer from training instability, producing unpleasant artifacts that hinder practical applications.

Recently, diffusion models [18, 37, 41, 43, 46, 47] have gained prominence as a promising alternative, especially with the advent of large-scale pre-trained text-to-image (T2I) models like StableDiffusion (SD) [15, 38, 43]. To adapt them to ISR reconstruction, DiffBIR [32] preprocesses images with traditional ISR networks before refining them with ControlNet-based [73] SD models. In contrast, FaithDiff [8] aligns the representations with LR images at each time step to balance fidelity and realism. However, given that T2I models inherently map abstract textual se-

manics to concrete image pixels, relying solely on LR images without semantic control may introduce distortions in the reconstructed content.

With this insight, researchers have increasingly focused on textual semantic fusion. For instance, PASD [68] leverages off-the-shelf high-level models to extract caption-style descriptions to guide reconstruction. SeeSR [62], on the other hand, highlights the superiority of tags, employing RAM [77] to extract them and integrating their semantic representations into SD. However, these extracted texts typically overlook fine-grained components (*e.g.* background), and the uniform semantic inputs across blocks of different depths constrain depth-specific representations [53]. As illustrated in Fig. 1(a), we apply different prompts to blocks at varying depths. The results indicate that low-level image attributes are determined by wide blocks, while narrow blocks focus on the semantics. Hence, the first challenge is *how to supplement missing fine-grained semantic components and realize customization at different blocks?*

In addition to abstract text-level semantics, recent research has also explored pixel-level guidance to address reconstruction ambiguity within the same regions caused by textual inputs. HolisDiP [50] employs Mask2Former [11] for semantic segmentation and embeds each pixel’s label with CLIP [40] for dense guidance fusion. SegSR [63] formulates a parallel diffusion framework for images and segmentation maps, controlling the diffusion process via cross-branch interaction. However, when objects with the same semantics aggregate into larger regions, it is challenging to accurately delineate the contours of each entity from segmentation maps, sparking the potential for multi-guidance aggregation. Hence, the second challenge is *what is the most expressive pixel-level guidance and how can they be appropriately integrated into the diffusion process?*

To tackle the challenges above, we propose a novel framework to further mine customized fine-grained semantics and expressive guidance for ISR (**MegaSR**). Specifically, for the first challenge, MegaSR extracts fine-grained semantics from the image itself and then maps them into distinct expressions at each block to realize customization. For the second challenge, we first conduct a preliminary experiment to identify the most expressive pixel-level guidance. As illustrated in Fig. 1(b), we employ paired guidance with the same semantics but contradictory structures to Uni-ControlNet [78] each time and evaluate the relative impact of these guidance signals. By comparing six types of guidance, we identify the HED edge maps, depth maps, and segmentation maps as the most effective ones. HED edge maps are highly discriminative, enabling precise localization of critical structures and details within regions of the same semantics, while depth maps and segmentation maps provide rich multi-dimensional semantic priors. Thus, MegaSR first enhances the corresponding guid-

ance extractors with degradation-aware capabilities. Next, a multi-stage guidance aggregation module is introduced to fuse depth and segmentation maps into comprehensive representations, which then collaborate with HED edge maps to exert precise control over the diffusion process, facilitating rich and structurally consistent detail generation.

Our main contributions can be summarized as follows:

- We propose MegaSR, a novel framework that mines customized semantics and expressive guidance to unleash the powerful priors of T2I models for advanced ISR.
- We develop an effective customized image semantics mining module to supplement distinct fine-grained semantics to each block for enhanced context-aware ISR.
- We experimentally evaluate the impact of different guidance signals and design a multi-stage guidance aggregation module to progressively fuse the most effective ones, providing precise signals to the T2I models for ISR.
- Extensive experiments demonstrate that MegaSR reconstructs images with superior semantic richness and structural consistency.

## 2. Related Work

### 2.1. Image Super Resolution

Reconstructing HR images from degraded LR inputs remains a challenge in ISR. Early research [10, 12, 14, 28, 33, 35, 49], represented by SRCNN [13], focuses on end-to-end ISR models that utilize deep networks (*e.g.* CNN [23], RNN [70], Transformer [52]) as the backbone architecture. They typically synthesize LR-HR image pairs with pre-defined degradations (*e.g.* bicubic downsampling) and are optimized with fidelity-focused objectives (*e.g.* L1, MSE Loss). Despite demonstrating superiority in metrics like PSNR and SSIM, these approaches often result in over-smoothed reconstructions.

Recent advancements [9, 24, 56, 75] in ISR have incorporated Generative Adversarial Networks (GANs) [16] to integrate high-level priors into the reconstruction. They typically adopt pre-trained ISR models as generators and introduce discriminator networks for adversarial training, gradually refining texture and enhancing perceptual quality. However, due to the inherent instability [2, 4, 36] during training, GANs often introduce artifacts and structural distortions to the outcomes, degrading image quality. Beyond improvements in model architectures and training strategies, researchers have also explored data synthesis techniques to better simulate real-world degradations. Notable efforts include collecting LR-HR datasets by varying camera lens zoom [5] and simulating real-world degradations through random combinations of various degradation processes [57, 71]. More recently, the widely used DDPM [18] has provided novel insights [67] for ISR tasks.

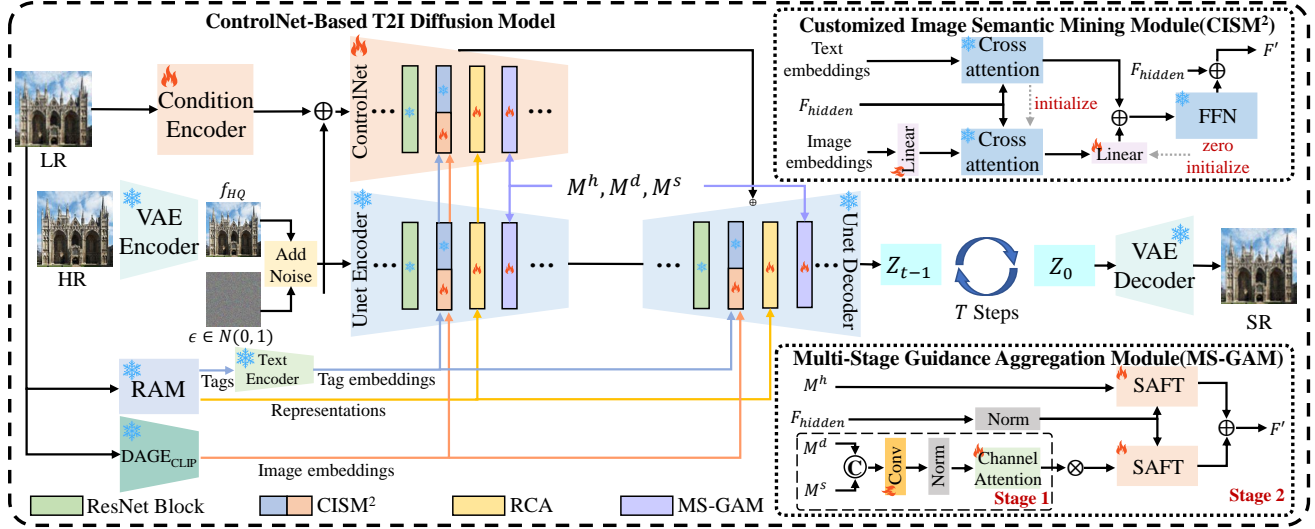


Figure 2. Overview of the proposed MegaSR. MegaSR extracts image embeddings using DAGE<sub>CLIP</sub>, which are then transformed into customized fine-grained semantic representations via CISM<sup>2</sup> at each block. Next, DAGE<sub>HED</sub>, DAGE<sub>DEP</sub>, and DAGE<sub>SEG</sub> are employed to extract HED edge maps  $M^h$ , depth maps  $M^d$ , and segmentation maps  $M^s$ , respectively. These guidance signals are injected into the ControlNet-based T2I diffusion model via MS-GAM, facilitating the reconstruction of semantically rich and structurally consistent images.

## 2.2. Diffusion-based Image Super Resolution

Inspired by GANs [16], researchers [6, 7, 20, 34, 44, 51, 76, 79, 80] have increasingly sought models with stronger prior knowledge and improved training stability. Diffusion models [18, 37, 41, 43, 46, 47], as a novel generative approach, have gained prominence due to pre-training on large-scale datasets with billions of image-text pairs.

Recently, several research [3, 26, 39, 45, 48, 55, 69] has explored the potential of pre-trained diffusion models (e.g. StableDiffusion (SD)) for ISR. StableSR [55] introduces a time-aware encoder to fine-tune the SD model, while DiffBIR [32] preprocesses the inputs before refining them with the ControlNet-based [73] SD model. FaithDiff [8] achieves LR-consistent reconstruction by training an alignment module to align with LR images at each timestep. Besides, high-level semantics is also an effective catalyst during diffusion. PASD [68] stimulates diffusion priors with caption-style descriptions extracted by off-the-shelf models (e.g. ResNet [17], YOLO [42], BLIP [27]). In contrast, SeeSR [62] highlights tags as more effective than captions, enhancing reconstruction with RAM [77]. Textual semantics may introduce ambiguity for ISR. Hence, HoliSDiP [50] embeds semantic segmentation with CLIP for dense semantic guidance, while SegSR [63] adopts a parallel diffusion framework for semantic segmentation and image reconstruction. However, it is challenging to delineate the contours of entities with the same semantics when aggregated into larger regions. Thus, identifying the most effective high-level guidance is crucial for advancing ISR.

## 3. Method

### 3.1. Preliminary

In this work, we use Stable Diffusion (SD) [43] as the base diffusion model. SD is fundamentally a Markov chain of  $T$  steps, which comprises a forward process and a reverse process. The forward process progressively adds noise with variance coefficient  $1 - \alpha_t$  to the latent representations  $z_{t-1}$ , which can be formulated and further derived as:

$$\begin{aligned} z_t &= \sqrt{\alpha_t} z_{t-1} + \sqrt{1 - \alpha_t} \epsilon_{t-1}, \\ z_t &= \sqrt{\bar{\alpha}_t} z_0 + \sqrt{1 - \bar{\alpha}_t} \epsilon, \end{aligned} \quad (1)$$

where  $\epsilon \sim \mathcal{N}(0, 1)$  and  $\bar{\alpha}_t = \prod_{i=0}^t \alpha_i$ . The reverse process starts with pure noise  $z_t$ , and progressively estimates the noise  $\epsilon$  conditioned on  $c$  through the pretrained  $\theta$ -parameterized denoising network  $\epsilon_\theta$ . The optimization objective can be described as:

$$\mathcal{L}_{LDM} = \mathbb{E}_{z_t, c, t, \epsilon} [\|\epsilon - \epsilon_\theta(z_t, c, t)\|_2^2]. \quad (2)$$

### 3.2. Framework Overview

The framework of our proposed MegaSR is shown in Fig. 2. Different from general ISR methods that merely supplement abstract textual semantics and one type of pixel-level guidance, MegaSR enhances each block with customized fine-grained image semantics and incorporates multi-dimensional aggregated guidance to improve semantical richness and structural consistency.

In practice, high-level guidance extractors are typically designed to tackle common inputs. Although some methods incorporate low-level data augmentation during pretraining,

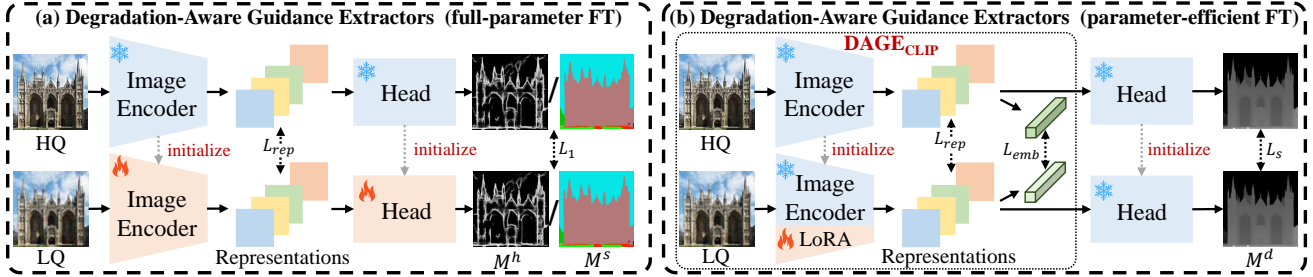


Figure 3. The fine-tuning process of our DAGEs. (a) For edge detection and semantic segmentation, we apply full-parameter fine-tuning to HED [64] and MaskDINO [25]. (b) For depth estimation [65] and image embedding extraction [40], we accelerate the process using parameter-efficient fine-tuning. Both the intermediate representations and final outputs are expected to align with those of the HR branch.

they often struggle to match real-world degradations, which is often neglected by existing methods. Following SeeSR, to equip these extractors with robust degradation-aware capabilities, we impose constraints not only on the final outputs but also on intermediate representations, which will be detailed introduced in Sec. 3.3. We define the fine-tuning objective for these DAGEs as follows:

$$\mathcal{L}_{DAGEs} = \mathcal{L}_{rep} + \mathcal{L}_{out}. \quad (3)$$

Based on the powerful multimodal projection and degradation-aware capabilities of DAGE<sub>CLIP</sub>, we encode LR images into the same high-dimensional embedding space as textual tags. Then we employ independent semantics projection to derive block-wise customized semantics from these embeddings and ultimately fused with textual ones. The details will be introduced in Sec. 3.4.

For guidance injection, we first extract these signals with DAGE<sub>HED</sub>, DAGE<sub>DEP</sub>, and DAGE<sub>SEG</sub>. Then we interact and aggregate depth and segmentation maps along the channel dimension to generate multi-dimensional guidance representations. Finally, the representations and HED edge maps are separately injected to modulate the latent representations of the SD model, serving as complementary control signals. Further details are presented in Sec. 3.5.

The overall training objective of the ControlNet-based T2I diffusion model in MegaSR can be formulated as:

$$\min_{\theta} \mathcal{L} = \mathbb{E}_{z_t, s, g, t, \epsilon} [\|\epsilon - \epsilon_{\theta}(z_t, s, g, t)\|_2^2], \quad (4)$$

where  $s$  and  $g$  denote the customized semantics and guidance, respectively.

### 3.3. Degradation-Aware Guidance Extractors

Inspired by SeeSR, we employ two fine-tuning strategies tailored to different model architectures, equipping them with degradation-aware capabilities.

Firstly, we apply full-parameter fine-tuning to the commonly used edge detection model (e.g. HED [64]) and semantic segmentation model (e.g. MaskDINO [25]). As shown in Fig. 3(a), the HR image  $I_{hr}$  is passed through a

frozen guidance extractor to extract the representation embeddings  $F_{hr}^{eh}/F_{hr}^{es}$  and guidance  $I_{hr}^h/I_{hr}^s$ . Similarly, the LR image  $I_{lr}$  goes through the same process, except that both the backbone and the head are trainable and initialized with that of the HR counterparts. To enhance robustness of DAGEs, we force both the representation embeddings and the outputs from the LR branch to closely align with that of the HR branch. The training objective is as follows:

$$\begin{aligned} \mathcal{L}_{hed} &= \mathcal{L}_1(F_{hr}^{eh}, F_{lr}^{eh}) + \alpha \mathcal{L}_1(I_{hr}^h, I_{lr}^h), \\ \mathcal{L}_{seg} &= \mathcal{L}_1(F_{hr}^{es}, F_{lr}^{es}) + \beta \mathcal{L}_1(I_{hr}^s, I_{lr}^s), \end{aligned} \quad (5)$$

where  $\alpha$  and  $\beta$  are balance factors,  $F_{lr}^{eh}, F_{lr}^{es}$  denote representation embeddings of the HED model and MaskDINO,  $I_{lr}^h$  and  $I_{lr}^s$  are edge maps and segmentation maps of the LR branch, and  $\mathcal{L}_1$  is mean absolute error (MAE) loss.

Furthermore, to accelerate the fine-tuning process, we adopt the parameter-efficient fine-tuning strategy for the depth estimation model (e.g. DepthAnythingV2 [65]) and CLIP [40]. As illustrated in Fig. 3(b), LoRA ( $r=8$ ) is integrated into the backbone while keeping all other parameters frozen. Since CLIP does not include the head, the training objective function is as follows:

$$\begin{aligned} \mathcal{L}_{dep} &= \mathcal{L}_1(F_{hr}^{ed}, F_{lr}^{ed}) + \gamma \mathcal{L}_s(I_{hr}^d, I_{lr}^d), \\ \mathcal{L}_{clip} &= \mathcal{L}_1(F_{hr}^{ec}, F_{lr}^{ec}) + \sum_{i=1}^N \mathcal{L}_1(F_{hr}^i, F_{lr}^i), \end{aligned} \quad (6)$$

where  $\gamma$  is also a balance factor,  $F_{hr}^{ed}$  and  $F_{lr}^{ec}$  denote representation embeddings of the DepthAnythingV2 and CLIP,  $I_{hr}^d$  and  $I_{lr}^d$  are the depth map of the HR and LR branch,  $F^i$  denotes the intermediate features of ViT, and  $\mathcal{L}_s$  is scale-invariant logarithmic (SILog) loss. With effective fine-tuning strategies, MegaSR incorporates more precise pixel-level guidance from DAGEs, significantly improving the structural consistency of reconstructed results.

### 3.4. Customized Image Semantics Mining Module

The Customized Image Semantic Mining Module (CISM<sup>2</sup>) is proposed to supplement fine-grained semantic represen-

tations tailored to each block. The structure of the proposed CISM<sup>2</sup> is illustrated in the top-right corner of Fig. 2(c).

Specifically, CISM<sup>2</sup> consists of two components: a frozen textual abstract semantics fusion branch (text branch for short) and a trainable image concrete semantics mining branch (image branch for short). The text branch directly employs the cross-attention (CA) module from the original SD model. In the image branch, we first adopt DAGE<sub>CLIP</sub>, fine-tuned in Sec. 3.3, to extract image embeddings from LR images. The embeddings are then passed through a projection layer to implement mapping from the CLIP image embedding space to the diffusion text embedding space, obtaining  $F_{lr}^l$ . Next,  $F_{lr}^l$  is processed by a frozen CA module, initialized with that in the text branch, to allow interaction with the diffusion latent representations. Finally, the block-wise customized semantic outcome  $F'$  is obtained as:

$$\begin{aligned} F_{lr}^l &= \text{Linear}(\text{DAGE}_{\text{CLIP}}(I_{lr})), \\ F^i &= \text{CA}(F_{lr}^l, F_{\text{hidden}}), \\ F' &= \text{FFN}(\text{Linear}(F^i) + F^t) + F_{\text{hidden}}, \end{aligned} \quad (7)$$

where  $F^i$  and  $F^t$  denotes the image and textual semantics,  $F_{\text{hidden}}$  denotes the latent representations of the SD model,  $\text{Linear}(\cdot)$  denotes fully connected layers, and  $\text{FFN}(\cdot)$  denotes the feedforward network.

Notably, CISM<sup>2</sup> is both simple and effective, achieving superior performance with minimal additional parameters. Moreover, the customized block-wise design allows the same image embeddings to be transformed into distinct semantic representations at different blocks. Compared to existing methods where the mapping is performed externally, CISM<sup>2</sup> offers greater flexibility and adaptability.

### 3.5. Multi-Stage Guidance Aggregation Module

Given that the HED edge maps capture fine-grained internal contours of semantic objects, while depth and segmentation maps provide complementary vertical and horizontal guidance within the channel dimension, we propose a Multi-Stage Guidance Aggregation Module (MS-GAM) to better exploit these multi-dimensional cues. MS-GAM first integrates the depth and semantic segmentation maps, then jointly modulates the latent representations of the SD model with the HED edge maps.

As shown in the bottom-right corner of Fig. 2(c), in the first stage, we concatenate the depth  $M^d$  and segmentation map  $M^s$  to obtain  $M^c$ , followed by a convolutional block to extract shallow features  $F^s$ . To efficiently enhance the interaction between depth and segmentation signals, we pass  $F^s$  through a channel attention mechanism, which then yields the fine-grained multi-dimensional guidance  $F^r$  as:

$$\begin{aligned} M^c &= \text{Concat}(M^d, M^s), \\ F^c &= \text{ChannelAttn}(\text{Conv}(M^c)), \\ F^r &= F^c \otimes M^c, \end{aligned} \quad (8)$$

where  $\text{ChannelAttn}(\cdot)$  denotes the channel attention mechanism and  $\otimes$  denotes element-wise multiplication.

In the second stage, the HED edge maps  $M^h$  and multi-dimensional guidance  $F^r$  are processed by separate Semantic Adaptive Feature Transformation Blocks (SAFT) to modulate the latent representations within the SD models, obtaining transformed representations  $F'$  as:

$$\begin{aligned} F^h &= \text{SAFT}(\text{Norm}(F_{\text{hidden}}), M^h), \\ F^m &= \text{SAFT}(\text{Norm}(F_{\text{hidden}}), F^r), \\ F' &= F^h + F^m. \end{aligned} \quad (9)$$

By integrating HED edge maps, depth maps, and segmentation maps within the proposed MS-GAM, the SD model is enriched with fine-grained, multi-dimensional guidance, improving the preservation of fine details in the reconstructed outcomes. More comparative results of guidance signals are presented in Appendix A.

## 4. Experiments

### 4.1. Experimental Settings

**Datasets.** Following the standard training settings proposed by SeeSR [62] and HoliSDiP [50], we used the LS-DIR [29] dataset and the first 10,000 face images from FFHQ [21] for training, combining with the degradation pipeline from Real-ESRGAN [57] to synthesize LR-HR image pairs. For evaluation, we assessed the effectiveness of our method on RealSR [5], DrealSR [60], DIV2K-Val [1], and DPED-iPhone [19].

**Implementation Details.** We adopted the SD-2-base<sup>1</sup> model as our base model and collaborated with the DAPE-equipped RAM to extract image tags and semantic representations. Following the method described in Sec. 3.3, we fine-tuned the HED model [64] for edge detection and MaskDINO [25] for semantic segmentation. For depth estimation and image embedding extraction, we employed the LoRA (r=8) method for parameter-efficient fine-tuning of DepthAnythingV2 [65] and CLIP ViT-H/14<sup>2</sup>. Details of the fine-tuning settings are illustrated in Appendix B.

The whole ControlNet-based T2I diffusion model was trained for 200K steps using the Adam optimizer, along with the batch size and learning rate of 16 and  $2.5 \times 10^{-5}$ , respectively. The training process was conducted on 2 NVIDIA RTX A100 40G GPUs, with  $512 \times 512$  resolution LR-HR image pairs. For inference, we employed DDPM sampling and LRE strategy with 50 timesteps.

**Evaluation Metrics.** To enable a comprehensive comparison with contemporary methods, we adopted seven widely used evaluation metrics, including a wide range of reference-based and non-reference ones. Specifically, for

<sup>1</sup><https://huggingface.co/stabilityai/stable-diffusion-2-base>

<sup>2</sup><https://github.com/openai/CLIP>

Table 1. Quantitative comparison of contemporary ISR methods on both synthetic and real-world datasets. The best, second-best, and third-best results are highlighted in **red**, **blue**, and **black**, respectively. † indicates our reproduced version due to certain flaws in the original code. The proposed MegaSR achieves leading performance across multiple non-reference metrics, and is competitive in reference-based scenarios among diffusion-based methods, demonstrating its superiority.

Dataset	Metric	GAN-based					Diffusion-based							
		BSRGAN	Real-ESRGAN	LDL	FeMaSR	DASR	StableSR	SinSR	DiffBIR	SeeSR	OSDiff	HoliSDiP†	FaithDiff	MegaSR
RealSR	PSNR↑	<b>24.75</b>	24.15	23.76	23.51	<b>25.40</b>	23.14	24.48	23.91	23.60	23.59	23.70	<b>24.91</b>	23.49
	SSIM↑	<b>0.7401</b>	<b>0.7363</b>	0.7300	0.7088	<b>0.7458</b>	0.6796	0.7076	0.6220	0.6947	0.7071	0.6994	0.7129	0.6903
	LPIPS↓	<b>0.2656</b>	<b>0.2710</b>	0.2750	0.2937	0.3134	0.3000	0.3186	0.3732	0.3007	0.2920	0.2977	<b>0.2562</b>	0.3072
	NIQE↓	5.6348	5.8027	5.9916	5.7673	6.5455	5.9755	6.2835	6.0788	<b>5.4008</b>	5.6341	<b>5.3884</b>	6.0413	<b>5.3795</b>
	MANIQA↑	0.3758	0.3737	0.3794	0.3629	0.2470	0.4244	0.3997	0.5022	<b>0.5437</b>	0.4711	<b>0.5290</b>	0.3907	<b>0.5574</b>
	MUSIQ↑	63.2861	60.3665	60.9249	59.0588	41.2030	65.6786	60.5986	64.9021	<b>69.8200</b>	<b>69.0892</b>	68.9540	64.2661	<b>70.0251</b>
	CLIQQA↑	0.5116	0.4491	0.4559	0.5406	0.3202	0.6184	0.6280	0.6507	<b>0.6700</b>	<b>0.6693</b>	0.6639	0.5857	<b>0.6790</b>
DIV2K-Val	PSNR↑	<b>22.79</b>	<b>22.60</b>	22.18	21.32	<b>22.75</b>	21.62	22.51	21.83	21.97	<b>22.05</b>	22.19	22.49	22.05
	SSIM↑	0.5908	<b>0.5986</b>	<b>0.5926</b>	0.5536	<b>0.5924</b>	0.5340	0.5675	0.5033	0.5673	0.5735	0.5742	0.5645	0.5664
	LPIPS↓	0.3351	<b>0.3112</b>	0.3256	0.3126	0.3543	0.3125	0.3244	0.3763	0.3194	<b>0.2942</b>	0.3248	<b>0.2640</b>	0.3157
	NIQE↓	4.7513	<b>4.6787</b>	4.8557	<b>4.7415</b>	5.0273	4.7644	6.0022	5.1361	4.8095	<b>4.7081</b>	4.9206	5.1585	4.8258
	MANIQA↑	0.3532	0.3790	0.3727	0.3443	0.3164	0.4198	0.4225	<b>0.5231</b>	<b>0.5036</b>	0.4411	0.4848	0.3659	<b>0.5074</b>
	MUSIQ↑	61.1963	61.0566	60.0398	60.8291	55.1963	65.7148	62.7473	66.3764	<b>68.6699</b>	<b>67.9716</b>	67.5952	65.1001	<b>68.7602</b>
	CLIQQA↑	0.5247	0.5277	0.5180	0.5998	0.5036	0.6770	0.6482	<b>0.6840</b>	<b>0.6936</b>	0.6680	0.6635	0.6049	<b>0.6892</b>
DrealSR	PSNR↑	<b>26.39</b>	26.28	25.97	24.85	<b>27.24</b>	25.73	25.84	24.99	26.01	25.89	25.48	<b>26.50</b>	25.74
	SSIM↑	0.7739	<b>0.7767</b>	<b>0.7839</b>	0.7247	<b>0.7995</b>	0.7178	0.7151	0.6035	0.7330	0.7546	0.7446	0.7240	0.7367
	LPIPS↓	<b>0.2858</b>	<b>0.2819</b>	<b>0.2792</b>	0.3157	0.3099	0.3262	0.3701	0.4662	0.3485	0.2967	0.3167	0.2989	0.3258
	NIQE↓	<b>6.5400</b>	6.6929	7.1427	<b>5.9096</b>	7.5857	6.6791	6.9613	6.6915	6.9710	<b>6.4197</b>	6.6601	6.8838	6.6276
	MANIQA↑	0.3404	0.3440	0.3429	0.3165	0.2808	0.3855	0.3838	<b>0.4935</b>	<b>0.5290</b>	0.4655	0.4781	0.3666	<b>0.5098</b>
	MUSIQ↑	57.1682	54.2724	53.9454	53.7099	42.4116	59.8183	55.4730	60.4019	<b>64.4534</b>	<b>64.7006</b>	63.1544	59.1474	<b>64.1473</b>
	CLIQQA↑	0.5099	0.4520	0.4477	0.5638	0.3812	0.6241	0.6394	0.6483	<b>0.6816</b>	<b>0.6966</b>	0.6450	0.5892	<b>0.6853</b>
DPED-iPhone	NIQE↓	<b>6.4908</b>	6.8455	6.9554	<b>6.6287</b>	6.6843	6.7322	7.9803	7.3028	6.7261	<b>6.3652</b>	6.7430	6.6519	6.7751
	MANIQA↑	0.3136	0.3036	0.3133	0.3570	0.2557	0.3567	0.3569	<b>0.4573</b>	<b>0.4581</b>	0.4425	0.4037	0.3334	<b>0.4653</b>
	MUSIQ↑	45.8906	42.4342	43.6455	49.9494	32.6858	51.8923	46.7074	54.8280	<b>57.6794</b>	<b>56.3909</b>	55.1995	52.1251	<b>56.3767</b>
	CLIQQA↑	0.4022	0.3382	0.3535	0.5307	0.2826	0.4920	0.5743	0.5770	<b>0.6077</b>	<b>0.5927</b>	0.5885	0.4616	<b>0.6201</b>

image fidelity assessment, we utilized the reference-based metrics, including PSNR and SSIM [59], with the calculations conducted in the YCbCr space. For perceptual quality, we employed the remaining five metrics, including LPIPS [74] as reference-based metrics, and NIQE [72], MANIQA [66], MUSIQ [22], and CLIPIQA [54] as non-reference ones. Notably, all evaluations were conducted with the IQA-Pytorch<sup>3</sup> project to ensure fairness.

**Compared Methods.** We compared two categories of ISR methods: GAN-based and diffusion-based approaches. Specifically, the GAN-based methods include BSRGAN [71], Real-ESRGAN [57], LDL [30], FeMaSR [6], and DASR [31], while the diffusion model-based methods comprise StableSR [55], SinSR [58], DiffBIR [32], SeeSR [62], OSDiff [61], HoliSDiP [50], and FaithDiff [8]. We used the publicly released codes and models of the competing methods for testing.

## 4.2. Comparison with State-of-the-Arts

**Quantitative Comparison.** We present a comprehensive quantitative comparison between the proposed MegaSR and several state-of-the-art methods across the five synthetic and real-world datasets in Tab. 1. The following conclusions can be drawn. (1) MegaSR consistently outperforms competing methods across all five datasets, particularly excelling in human perception-based evaluation metrics, including MANIQA [66], MUSIQ [22], and CLIPIQA [54]. Notably, MegaSR surpasses the second-best method by 2.5%

in MANIQA and 2% in CLIPIQA on RealSR and DEPE-iPhone dataset respectively, highlighting its advantage in perceptual image quality. (2) MegaSR also demonstrates competitive performance among diffusion-based methods in terms of reference-based metrics: PSNR, SSIM, LPIPS, which demonstrates its ability to reconstruct high-fidelity images while enhancing perceptual realism through the powerful T2I model. (3) In contrast, GAN-based methods, including BSRGAN [71], RealESRGAN [57], LDL [30], FeMaSR [6], and DASR [31], excel in traditional reference-based metrics but struggle with the perception-driven ones.

The observations above reinforce a well-established argument in prior research [74]: traditional reference-based metrics often fail to capture human visual preferences, as they overlook the naturalness and realism of images. Moreover, HR images themselves may contain imperfections, further limiting their reliability in real-world scenarios. In contrast, diffusion-based methods prioritize perceptual realism over strict fidelity, producing visually appealing and perceptually consistent results through diffusion priors.

**Qualitative Comparison.** Fig. 4 provides a qualitative visual comparison between the proposed method and existing ISR frameworks. Specifically, GAN-based methods typically tend to introduce unpleasant artifacts (column 3), while diffusion-based methods mitigate such artifacts but struggle to reconstruct fine-grained details, such as the window textures on the tower (row 2). Although SeeSR captures these details, it lacks structural neatness. In terms of semantic consistency (row 3), RealESRGAN [57],

<sup>3</sup><https://github.com/chaofengc/IQA-PyTorch>

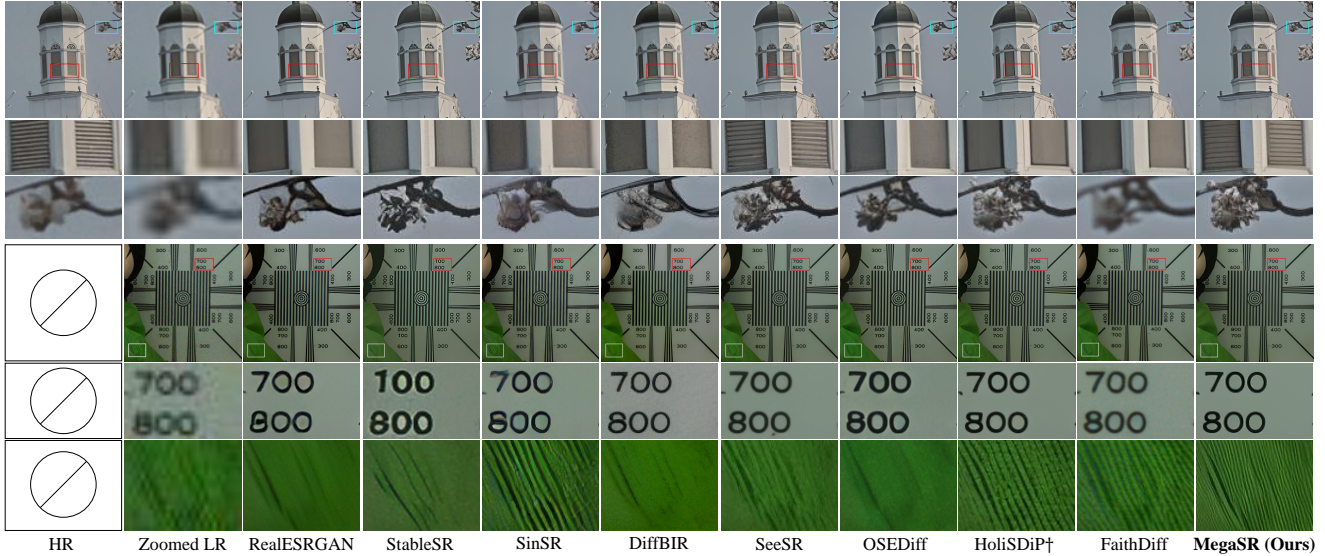


Figure 4. Qualitative comparisons of different ISR methods. MegaSR achieves superior accuracy and realism in terms of semantic preservation and structural consistency.

Table 2. Ablation study of DAGES. The best results are shown in **red**. GE denotes guidance extractors without fine-tuning.

Experiments	<i>RealSR</i>			
	PSNR $\uparrow$	MANIQA $\uparrow$	MUSIQ $\uparrow$	CLIPQA $\uparrow$
Ours w/ GE	23.2260	0.5483	68.9973	0.6751
Ours	<b>23.4909</b>	<b>0.5574</b>	<b>70.0252</b>	<b>0.6790</b>

SinSR [58], and DiffBIR [32] fail to preserve object semantics, while StableSR [55], SeeSR [62], OSEDiff [61], and HoliSDiP [50] exhibit noticeable texture distortions. FaithDiff [8], on the other hand, underperforms in clarity. In contrast, MegaSR effectively restores both precise texture details and semantic integrity, demonstrating advantages in both perceptual fidelity and semantic preservation.

In real-world scenarios, our method also demonstrates superior performance. For text reconstruction (row 5), RealESRGAN, StableSR, SinSR, DiffBIR, OSEDiff, and HoliSDiP typically introduce structural distortions, while SeeSR and FaithDiff struggle with clarity. When it comes to texture restoration (row 6), RealESRGAN, StableSR, DiffBIR, SeeSR, and OSEDiff generate over-smoothed outcomes, whereas SinSR, and HoliSDiP exhibit unnatural textures. And FaithDiff still exhibits potential in overall clarity. In comparison, MegaSR achieves superior accuracy and clarity in restoring structural and textual details. More comparative results are presented in Appendix C.

### 4.3. Ablation Studies

To validate the effectiveness and rationale of the proposed method, we conduct a series of in-depth ablation experiments from the perspectives of model designs and guidance.

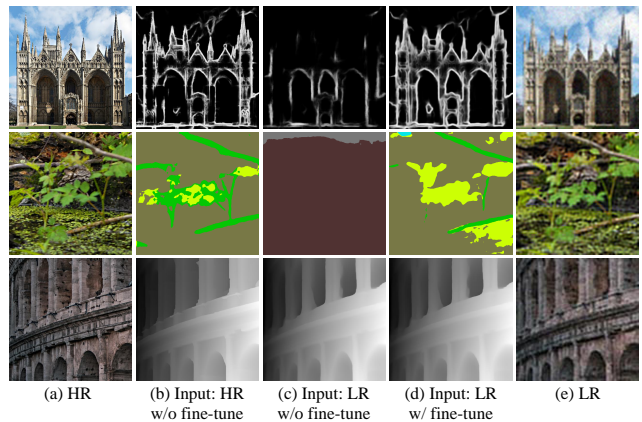


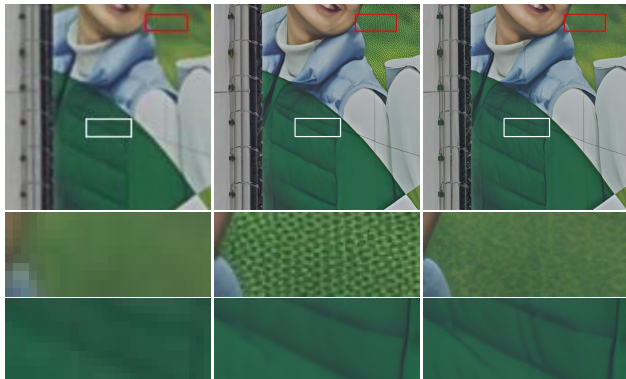
Figure 5. Visual comparison of high-level outputs before and after fine-tuning. The proposed DAGES tackle LR inputs as closely as possible to that of HR without fine-tuning.

**Effectiveness of the degradation-aware guidance extractors.** The primary objective of fine-tuning the guidance extractors is to improve their sensitivity to image degradation, enabling them to generate outputs more consistent with HR images. As illustrated in Tab. 2, our method outperforms the baseline across all fidelity-focused and quality-driven metrics.

To further evaluate the effectiveness of DAGES, we input both LR and HR images into the models before and after fine-tuning and compare the results. As shown in Fig. 5, except for DepthAnythingV2 [65], pre-trained models produce results that deviate considerably from HR images when processing LR inputs (column 3), indicating their limited robustness to image degradation. Fine-tuning significantly enhances their ability (column 4) to generate accurate guidance for diffusion-based super-resolution, ultimately improving overall reconstruction performance.

Table 3. Ablation study of CISM<sup>2</sup>. The best results are highlighted in **red**. CSIM<sup>2</sup> enables the proposed MegaSR to achieve the best visual quality.

Experiments	RealSR			
	PSNR $\uparrow$	MANIQA $\uparrow$	MUSIQ $\uparrow$	CLIPQA $\uparrow$
Ours w/o CISM <sup>2</sup>	<b>23.6411</b>	0.5371	69.3150	0.6553
Ours	23.4909	<b>0.5574</b>	<b>70.0252</b>	<b>0.6790</b>



(a) LR (b) Ours w/o CISM<sup>2</sup> (c) Ours

Figure 6. Visualization showing the effect of employing the proposed Customized Image Semantic Mining Module (CISM<sup>2</sup>). With the customized fine-grained image semantics learned from CISM<sup>2</sup>, MegaSR generates semantically correct content.

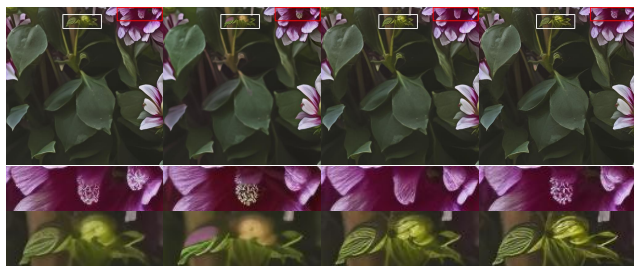
**Effectiveness of the customized image semantic mining module.** The proposed Customized Image Semantic Mining Module (CISM<sup>2</sup>) extracts fine-grained visual semantics and constructs specialized semantic representations at different blocks within the SD model. To evaluate its effectiveness, we remove the CISM<sup>2</sup> (**Ours w/o CISM<sup>2</sup>**) and compare the results with our method. As shown in Tab. 3, our method outperforms both baselines across quality-driven metrics, notably improving MANIQA [66] from 0.5371 to 0.5574, MUSIQ [22] from 69.3150 to 70.0252, and CLIPQA [54] from 0.6553 to 0.6790 on the RealSR dataset, while maintaining competitive results on other metrics.

Although the baseline models achieve better PSNR scores, as illustrated in Fig. 6, their reconstructed images exhibit unpleasant artifacts in fine details and excessive smoothing in certain regions, compromising overall realism. In contrast, our method achieves a balance between removing artifacts and preserving textures, demonstrating advantages in restoring fine details. These findings suggest that CISM<sup>2</sup> effectively enriches image-level contextual embeddings, complementing the abstract semantic information provided by text and enhancing reconstruction quality.

**Effectiveness of the multi-stage guidance aggregation module.** MS-GAM is proposed to incorporate high-level guidance into the diffusion process, enhancing structural consistency and spatial layout. To evaluate the contribution of different guidance signals, we conducted ablation experiments by selectively removing HED maps, depth

Table 4. Effectiveness of the proposed Multi-Stage Guidance Aggregation Module (MS-GAM). The best results are highlighted in **red**. H, D, and S denote HED edge maps, depth maps and segmentation map, respectively.

Experiments	RealSR			
	PSNR $\uparrow$	MANIQA $\uparrow$	MUSIQ $\uparrow$	CLIPQA $\uparrow$
Ours w/o (H & D & S)	<b>23.9221</b>	0.5213	68.3985	0.6621
Ours w/o (D & S)	23.9197	0.5390	68.6778	0.6555
Ours w/o H	23.8420	0.5291	68.9672	0.6606
Ours	23.4909	<b>0.5574</b>	<b>70.0252</b>	<b>0.6790</b>



(a) Ours w/o (H & D & S) (b) Ours w/o (D & S) (c) Ours w/o H (d) Ours

Figure 7. Visualization of different baseline methods and our proposed method. MS-GAM enables MegaSR to achieve superior performance in color reconstruction and texture enhancement.

maps, and segmentation maps within MS-GAM. As shown in Tab. 4, incorporating HED edge maps enhances realism while preserving fidelity, as reflected by the improvements in MANIQA and MUSIQ scores, with only a minor decrease in PSNR. Similarly, adding depth and segmentation maps also improve image quality, as evidenced by a clear increase in MUSIQ scores. Notably, integrating all guidance signals achieves the optimal balance between fidelity and realism, where a slight compromise in strict fidelity allows for the reconstruction of richer visual details.

Fig. 7 provides qualitative evidence supporting these findings. Incorporating HED maps improves overall smoothness, aligning with the quantitative results, but the absence of semantic guidance introduces color deviations in fine regions. Adding only these semantic guidance improves object reconstruction accuracy, but the texture details remain unnatural. Ultimately, integrating all three guidance signals allows the model to capture both high- and low-level attributes, enhancing texture reconstruction and significantly improving realism and detail preservation.

## 5. Conclusion and Limitation

We propose MegaSR, a novel real-world image super-resolution framework that leverages customized fine-grained image-level semantics at each block to stimulate generative priors of the SD models. Through experimental analysis, we identify HED edge maps, depth maps, and semantic segmentation maps as key guidance signals and fine-tune corresponding guidance extractors to align with ISR requirements. To further enhance performance, we design a

multi-stage aggregation strategy to seamlessly incorporate these multi-dimensional guidance signals into the diffusion process. Extensive experiments on both synthetic and real-world datasets demonstrate that MegaSR surpasses state-of-the-art models in terms of semantic richness and structural consistency of the reconstruction.

There are some limitations of MegaSR. First, under extreme degradation conditions, DAGEs may generate erroneous guidance, potentially misleading the diffusion process and compromising reconstruction. Second, MegaSR holds considerable potential for exploration in one-step ISR, aiming to achieve faster and better reconstruction. These challenges inspire further advancements in ISR.

## References

- [1] Eirikur Agustsson and Radu Timofte. NTIRE 2017 challenge on single image super-resolution: Dataset and study. In *CVPRW*, 2017. 5
- [2] Martín Arjovsky, Soumith Chintala, and Léon Bottou. Wasserstein GAN. *arXiv preprint arXiv:1701.07875*, 2017. 2
- [3] Chunyang Bi, Xin Luo, Sheng Shen, Mengxi Zhang, Huanjing Yue, and Jingyu Yang. Deedsr: Towards real-world image super-resolution via degradation-aware stable diffusion. *arXiv preprint arXiv:2404.00661*, 2024. 3
- [4] Andrew Brock, Jeff Donahue, and Karen Simonyan. Large scale GAN training for high fidelity natural image synthesis. In *ICLR*, 2019. 2
- [5] Jianrui Cai, Hui Zeng, Hongwei Yong, Zisheng Cao, and Lei Zhang. Toward real-world single image super-resolution: A new benchmark and a new model. In *ICCV*, 2019. 2, 5
- [6] Chaofeng Chen, Xinyu Shi, Yipeng Qin, Xiaoming Li, Xiaoguang Han, Tao Yang, and Shihui Guo. Real-world blind super-resolution via feature matching with implicit high-resolution priors. In *ACM MM*, 2022. 3, 6
- [7] Junsong Chen, Jincheng Yu, Chongjian Ge, Lewei Yao, Enze Xie, Zhongdao Wang, James T. Kwok, Ping Luo, Huchuan Lu, and Zhenguo Li. Pixart- $\alpha$ : Fast training of diffusion transformer for photorealistic text-to-image synthesis. In *ICLR*, 2024. 3
- [8] Junyang Chen, Jinshan Pan, and Jiangxin Dong. Faithdiff: Unleashing diffusion priors for faithful image super-resolution. In *CVPR*, 2025. 1, 3, 6, 7
- [9] Xiangyu Chen, Xintao Wang, Jiantao Zhou, Yu Qiao, and Chao Dong. Activating more pixels in image super-resolution transformer. In *CVPR*, 2023. 2
- [10] Zheng Chen, Yulun Zhang, Jinjin Gu, Linghe Kong, Xiaokang Yang, and Fisher Yu. Dual aggregation transformer for image super-resolution. In *ICCV*, 2023. 2
- [11] Bowen Cheng, Ishan Misra, Alexander G. Schwing, Alexander Kirillov, and Rohit Girdhar. Masked-attention mask transformer for universal image segmentation. In *CVPR*, 2022. 2
- [12] Tao Dai, Jianrui Cai, Yongbing Zhang, Shu-Tao Xia, and Lei Zhang. Second-order attention network for single image super-resolution. In *CVPR*, 2019. 1, 2
- [13] Chao Dong, Chen Change Loy, Kaiming He, and Xiaoou Tang. Learning a deep convolutional network for image super-resolution. In *ECCV*, 2014. 2
- [14] Chao Dong, Chen Change Loy, and Xiaoou Tang. Accelerating the super-resolution convolutional neural network. In *ECCV*, 2016. 1, 2
- [15] Patrick Esser, Sumith Kulal, Andreas Blattmann, Rahim Entezari, Jonas Müller, Harry Saini, Yam Levi, Dominik Lorenz, Axel Sauer, Frederic Boesel, Dustin Podell, Tim Dockhorn, Zion English, and Robin Rombach. Scaling rectified flow transformers for high-resolution image synthesis. In *ICML*, 2024. 1
- [16] Ian J. Goodfellow, Jean Pouget-Abadie, Mehdi Mirza, Bing Xu, David Warde-Farley, Sherjil Ozair, Aaron C. Courville, and Yoshua Bengio. Generative adversarial networks. *arXiv preprint arXiv:1406.2661*, 2014. 1, 2, 3
- [17] Kaiming He, Xiangyu Zhang, Shaoqing Ren, and Jian Sun. Deep residual learning for image recognition. In *CVPR*, 2016. 3
- [18] Jonathan Ho, Ajay Jain, and Pieter Abbeel. Denoising diffusion probabilistic models. In *NeurIPS*, 2020. 1, 2, 3
- [19] Andrey Ignatov, Nikolay Kobyshev, Radu Timofte, Kenneth Vanhoey, and Luc Van Gool. Dslr-quality photos on mobile devices with deep convolutional networks. In *ICCV*, 2017. 5
- [20] Younghyun Jo, Sejong Yang, and Seon Joo Kim. Srfrow-da: Super-resolution using normalizing flow with deep convolutional block. In *CVPR*, 2021. 3
- [21] Tero Karras, Samuli Laine, and Timo Aila. A style-based generator architecture for generative adversarial networks. *IEEE TPAMI*, 2021. 5
- [22] Junjie Ke, Qifei Wang, Yilin Wang, Peyman Milanfar, and Feng Yang. MUSIQ: multi-scale image quality transformer. In *ICCV*, 2021. 6, 8
- [23] Yann LeCun, Léon Bottou, Yoshua Bengio, and Patrick Haffner. Gradient-based learning applied to document recognition. *Proceedings of IEEE*, 1998. 2
- [24] Christian Ledig, Lucas Theis, Ferenc Huszar, Jose Caballero, Andrew Cunningham, Alejandro Acosta, Andrew P. Aitken, Alykhan Tejani, Johannes Totz, Zehan Wang, and Wenzhe Shi. Photo-realistic single image super-resolution using a generative adversarial network. In *CVPR*, 2017. 2
- [25] Feng Li, Hao Zhang, Huaizhe Xu, Shilong Liu, Lei Zhang, Lionel M. Ni, and Heung-Yeung Shum. Mask DINO: towards A unified transformer-based framework for object detection and segmentation. In *CVPR*, 2023. 4, 5
- [26] Haoying Li, Yifan Yang, Meng Chang, Huajun Feng, Zhihai Xu, Qi Li, and Yue-ting Chen. Srdiff: Single image super-resolution with diffusion probabilistic models. *arXiv preprint arXiv:2104.14951*, 2021. 3
- [27] Junnan Li, Dongxu Li, Caiming Xiong, and Steven C. H. Hoi. BLIP: bootstrapping language-image pre-training for unified vision-language understanding and generation. In *ICML*, 2022. 3
- [28] Wenbo Li, Xin Lu, Shengju Qian, and Jiangbo Lu. On efficient transformer-based image pre-training for low-level vision. In *IJCAI*, 2023. 1, 2

- [29] Yawei Li, Kai Zhang, Jingyun Liang, Jiezhong Cao, Ce Liu, Rui Gong, Yulun Zhang, Hao Tang, Yun Liu, Denis Deman-dolx, Rakesh Ranjan, Radu Timofte, and Luc Van Gool. LS-DIR: A large scale dataset for image restoration. In *CVPRW*, 2023. 5
- [30] Jie Liang, Hui Zeng, and Lei Zhang. Details or artifacts: A locally discriminative learning approach to realistic image super-resolution. In *CVPR*, 2022. 6
- [31] Jie Liang, Hui Zeng, and Lei Zhang. Efficient and degradation-adaptive network for real-world image super-resolution. In *ECCV*, 2022. 6
- [32] Xinqi Lin, Jingwen He, Ziyang Chen, Zhaoyang Lyu, Bo Dai, Fanghua Yu, Yu Qiao, Wanli Ouyang, and Chao Dong. Diff-bir: Toward blind image restoration with generative diffusion prior. In *ECCV*, 2024. 1, 3, 6, 7
- [33] Ding Liu, Bihan Wen, Yuchen Fan, Chen Change Loy, and Thomas S. Huang. Non-local recurrent network for image restoration. In *NeurIPS*, 2018. 2
- [34] Andreas Lugmayr, Martin Danelljan, Luc Van Gool, and Radu Timofte. Srflow: Learning the super-resolution space with normalizing flow. In *ECCV*, 2020. 3
- [35] Yiqun Mei, Yuchen Fan, and Yuqian Zhou. Image super-resolution with non-local sparse attention. In *CVPR*, 2021. 1, 2
- [36] Takeru Miyato, Toshiki Kataoka, Masanori Koyama, and Yuichi Yoshida. Spectral normalization for generative adversarial networks. In *ICLR*, 2018. 2
- [37] Alexander Quinn Nichol, Prafulla Dhariwal, Aditya Ramesh, Pranav Shyam, Pamela Mishkin, Bob McGrew, Ilya Sutskever, and Mark Chen. GLIDE: towards photorealistic image generation and editing with text-guided diffusion models. In *ICML*, 2022. 1, 3
- [38] Dustin Podell, Zion English, Kyle Lacey, Andreas Blattmann, Tim Dockhorn, Jonas Müller, Joe Penna, and Robin Rombach. SDXL: improving latent diffusion models for high-resolution image synthesis. In *ICLR*, 2024. 1
- [39] Yunpeng Qu, Kun Yuan, Kai Zhao, Qizhi Xie, Jinhua Hao, Ming Sun, and Chao Zhou. XPSR: cross-modal priors for diffusion-based image super-resolution. In *ECCV*, 2024. 3
- [40] Alec Radford, Jong Wook Kim, Chris Hallacy, Aditya Ramesh, Gabriel Goh, Sandhini Agarwal, Girish Sastry, Amanda Askell, Pamela Mishkin, Jack Clark, Gretchen Krueger, and Ilya Sutskever. Learning transferable visual models from natural language supervision. In *ICML*, 2021. 2, 4
- [41] Aditya Ramesh, Mikhail Pavlov, Gabriel Goh, Scott Gray, Chelsea Voss, Alec Radford, Mark Chen, and Ilya Sutskever. Zero-shot text-to-image generation. In *ICML*, 2021. 1, 3
- [42] Joseph Redmon, Santosh Kumar Divvala, Ross B. Girshick, and Ali Farhadi. You only look once: Unified, real-time object detection. In *CVPR*, 2016. 3
- [43] Robin Rombach, Andreas Blattmann, Dominik Lorenz, Patrick Esser, and Björn Ommer. High-resolution image synthesis with latent diffusion models. In *CVPR*, 2022. 1, 3
- [44] Chitwan Saharia, William Chan, Saurabh Saxena, Lala Li, Jay Whang, Emily L. Denton, Seyed Kamyar Seyed Ghasemipour, Raphael Gontijo Lopes, Burcu Karagol Ayan, Tim Salimans, Jonathan Ho, David J. Fleet, and Mohammad Norouzi. Photorealistic text-to-image diffusion models with deep language understanding. In *NeurIPS*, 2022. 3
- [45] Chitwan Saharia, Jonathan Ho, William Chan, Tim Salimans, David J. Fleet, and Mohammad Norouzi. Image super-resolution via iterative refinement. *IEEE TPAMI*, 2023. 3
- [46] Yang Song and Stefano Ermon. Generative modeling by estimating gradients of the data distribution. In *NeurIPS*, 2019. 1, 3
- [47] Yang Song, Jascha Sohl-Dickstein, Diederik P. Kingma, Abhishek Kumar, Stefano Ermon, and Ben Poole. Score-based generative modeling through stochastic differential equations. In *ICLR*, 2021. 1, 3
- [48] Lingchen Sun, Rongyuan Wu, Zhengqiang Zhang, Hongwei Yong, and Lei Zhang. Improving the stability of diffusion models for content consistent super-resolution. *arXiv preprint arXiv:2401.00877*, 2024. 3
- [49] Ying Tai, Jian Yang, and Xiaoming Liu. Image super-resolution via deep recursive residual network. In *CVPR*, 2017. 1, 2
- [50] Li-Yuan Tsao, Hao-Wei Chen, Hao-Wei Chung, Deqing Sun, Chun-Yi Lee, Kelvin C. K. Chan, and Ming-Hsuan Yang. Holisdip: Image super-resolution via holistic semantics and diffusion prior. *arXiv preprint arXiv:2411.18662*, 2024. 2, 3, 5, 6, 7
- [51] Aäron van den Oord, Oriol Vinyals, and Koray Kavukcuoglu. Neural discrete representation learning. In *NeurIPS*, 2017. 3
- [52] Ashish Vaswani, Noam Shazeer, Niki Parmar, Jakob Uszkoreit, Llion Jones, Aidan N. Gomez, Lukasz Kaiser, and Illia Polosukhin. Attention is all you need. In *NeurIPS*, 2017. 2
- [53] Andrey Voynov, Qinghao Chu, Daniel Cohen-Or, and Kfir Aberman. P+: extended textual conditioning in text-to-image generation. *arXiv preprint arXiv:2303.09522*, 2023. 2
- [54] Jianyi Wang, Kelvin C. K. Chan, and Chen Change Loy. Exploring CLIP for assessing the look and feel of images. In *AAAI*, 2023. 6, 8
- [55] Jianyi Wang, Zongsheng Yue, Shangchen Zhou, Kelvin C. K. Chan, and Chen Change Loy. Exploiting diffusion prior for real-world image super-resolution. *IJCV*, 2024. 3, 6, 7
- [56] Xintao Wang, Ke Yu, Shixiang Wu, Jinjin Gu, Yihao Liu, Chao Dong, Yu Qiao, and Chen Change Loy. ESRGAN: enhanced super-resolution generative adversarial networks. In *ECCVW*, 2018. 2
- [57] Xintao Wang, Liangbin Xie, Chao Dong, and Ying Shan. Real-esrgan: Training real-world blind super-resolution with pure synthetic data. In *ICCVW*, 2021. 2, 5, 6
- [58] Yufei Wang, Wenhan Yang, Xinyuan Chen, Yaohui Wang, Lanqing Guo, Lap-Pui Chau, Ziwei Liu, Yu Qiao, Alex C. Kot, and Bihan Wen. Sinsr: Diffusion-based image super-resolution in a single step. In *CVPR*, 2024. 6, 7
- [59] Zhou Wang, Alan C. Bovik, Hamid R. Sheikh, and Eero P. Simoncelli. Image quality assessment: from error visibility to structural similarity. *IEEE TIP*, 2004. 6
- [60] Pengxu Wei, Ziwei Xie, Hannan Lu, Zongyuan Zhan, Qixiang Ye, Wangmeng Zuo, and Liang Lin. Component

- divide-and-conquer for real-world image super-resolution. In *ECCV*, 2020. 5
- [61] Rongyuan Wu, Lingchen Sun, Zhiyuan Ma, and Lei Zhang. One-step effective diffusion network for real-world image super-resolution. In *NeurIPS*, 2024. 6, 7
- [62] Rongyuan Wu, Tao Yang, Lingchen Sun, Zhengqiang Zhang, Shuai Li, and Lei Zhang. Seesr: Towards semantics-aware real-world image super-resolution. In *CVPR*, 2024. 2, 3, 5, 6, 7
- [63] Jiahua Xiao, Jiawei Zhang, Dongqing Zou, Xiaodan Zhang, Jimmy S. J. Ren, and Xing Wei. Semantic segmentation prior for diffusion-based real-world super-resolution. *arXiv preprint arXiv:2412.02960*, 2024. 2, 3
- [64] Saining Xie and Zhuowen Tu. Holistically-nested edge detection. *IJCV*, 2017. 4, 5
- [65] Lihe Yang, Bingyi Kang, Zilong Huang, Zhen Zhao, Xiaogang Xu, Jiashi Feng, and Hengshuang Zhao. Depth anything V2. In *NeurIPS*, 2024. 4, 5, 7
- [66] Sidi Yang, Tianhe Wu, Shuwei Shi, Shanshan Lao, Yuan Gong, Mingdeng Cao, Jiahao Wang, and Yujiu Yang. MANIQA: multi-dimension attention network for no-reference image quality assessment. In *CVPRW*, 2022. 6, 8
- [67] Tao Yang, Peiran Ren, Xuansong Xie, and Lei Zhang. Synthesizing realistic image restoration training pairs: A diffusion approach. *arXiv preprint arXiv:2303.06994*, 2023. 2
- [68] Tao Yang, Rongyuan Wu, Peiran Ren, Xuansong Xie, and Lei Zhang. Pixel-aware stable diffusion for realistic image super-resolution and personalized stylization. In *ECCV*, 2024. 2, 3
- [69] Zongsheng Yue, Kang Liao, and Chen Change Loy. Arbitrary-steps image super-resolution via diffusion inversion. In *CVPR*, 2025. 3
- [70] Wojciech Zaremba, Ilya Sutskever, and Oriol Vinyals. Recurrent neural network regularization. *arXiv preprint arXiv:1409.2329*, 2014. 2
- [71] Kai Zhang, Jingyun Liang, Luc Van Gool, and Radu Timofte. Designing a practical degradation model for deep blind image super-resolution. In *ICCV*, 2021. 2, 6
- [72] Lin Zhang, Lei Zhang, and Alan C. Bovik. A feature-enriched completely blind image quality evaluator. *IEEE TIP*, 2015. 6
- [73] Lvmin Zhang, Anyi Rao, and Maneesh Agrawala. Adding conditional control to text-to-image diffusion models. In *ICCV*, 2023. 1, 3
- [74] Richard Zhang, Phillip Isola, Alexei A. Efros, Eli Shechtman, and Oliver Wang. The unreasonable effectiveness of deep features as a perceptual metric. In *CVPR*, 2018. 6
- [75] Wenlong Zhang, Yihao Liu, Chao Dong, and Yu Qiao. Ranksrgan: Super resolution generative adversarial networks with learning to rank. *IEEE TPAMI*, 2022. 2
- [76] Yi Zhang, Xiaoyu Shi, Dasong Li, Xiaogang Wang, Jian Wang, and Hongsheng Li. A unified conditional framework for diffusion-based image restoration. In *NeurIPS*, 2023. 3
- [77] Youcai Zhang, Xinyu Huang, Jinyu Ma, Zhaoyang Li, Zhaochuan Luo, Yanchun Xie, Yuzhuo Qin, Tong Luo, Yaqian Li, Shilong Liu, Yandong Guo, and Lei Zhang. Recognize anything: A strong image tagging model. In *CVPR*, 2024. 2, 3
- [78] Shihao Zhao, Dongdong Chen, Yen-Chun Chen, Jianmin Bao, Shaozhe Hao, Lu Yuan, and Kwan-Yee K. Wong. Uni-controlnet: All-in-one control to text-to-image diffusion models. In *NeurIPS*, 2023. 2
- [79] Yang Zhao, Yu-Chuan Su, Chun-Te Chu, Yandong Li, Marius Renn, Yukun Zhu, Changyou Chen, and Xuhui Jia. Rethinking deep face restoration. In *CVPR*, 2022. 3
- [80] Shangchen Zhou, Kelvin C. K. Chan, Chongyi Li, and Chen Change Loy. Towards robust blind face restoration with codebook lookup transformer. In *NeurIPS*, 2022. 3
- [81] Yupeng Zhou, Zhen Li, Chun-Le Guo, Song Bai, Ming-Ming Cheng, and Qibin Hou. Srformer: Permuted self-attention for single image super-resolution. In *ICCV*, 2023. 1